

Article

Calculation of Building Heat Losses through Slab-on-Ground Structures Based on Soil Temperature Measured In Situ

Iwona Pokorska-Silva ¹, Marta Kadela ^{2,*} , Bożena Orlik-Koźdoń ¹ and Lidia Fedorowicz ³

¹ Faculty of Civil Engineering, Silesian University of Technology, 44-100 Gliwice, Poland; iwona.pokorska-silva@polsl.pl (I.P.-S.); bozena.orlik-kozdon@polsl.pl (B.O.-K.)

² Building Research Institute (ITB), 00-611 Warsaw, Poland

³ Civil Engineering and Applied Arts, Faculty of Architecture, University of Technology, 40-555 Katowice, Poland; lidiafedorowicz@gmail.com

* Correspondence: m.kadela@itb.pl; Tel.: +48-603-60-12-48

Abstract: The article aims to assess the effects of soil temperature measured in situ on the heat loss analyses of a building. Numerical analyses and in situ measurements of soil temperature profiles for real conditions under a residential building (profile I) in Poland and under the area outside the building (profile II) were performed. Based on the measurement results, a proprietary geometric model of the partition was proposed. The heat flux and heat flow results obtained for reliable models are 4.9% and 6.9% higher compared to a model based on a typical meteorological year for the wall–foundation system and 10.0% and 10.1% higher for the slab-on-ground structure for profile I. The adoption of temperatures from the area outside the building as the boundary condition (profile II) results in greater differences between the obtained results. The difference in heat flow obtained in the numerical analyses for profiles I and II is about 2 W/m², both for the wall–foundation system and for the slab-on-ground structure calculations. The adoption of temperatures for the ground outside the building led to overestimation in the heat flux calculations, this being due to lower temperatures in these particular layers of the ground.

Keywords: ground temperature; ground profile; temperature measurement; heat flux; heat loss



Citation: Pokorska-Silva, I.; Kadela, M.; Orlik-Koźdoń, B.; Fedorowicz, L. Calculation of Building Heat Losses through Slab-on-Ground Structures Based on Soil Temperature Measured In Situ. *Energies* **2022**, *15*, 114. <https://doi.org/10.3390/en15010114>

Academic Editors: Sergio Ulgiati, Marco Casazza and Pedro L. Lomas

Received: 12 November 2021

Accepted: 23 December 2021

Published: 24 December 2021

Publisher's Note: MDPI stays neutral with regard to jurisdictional claims in published maps and institutional affiliations.



Copyright: © 2021 by the authors. Licensee MDPI, Basel, Switzerland. This article is an open access article distributed under the terms and conditions of the Creative Commons Attribution (CC BY) license (<https://creativecommons.org/licenses/by/4.0/>).

1. Introduction

Due to the growing necessity to reduce energy consumption [1,2], it is important to search for the most effective energy-saving solutions and to adopt efficient energy consumption strategies [3]. Related to this is heat gain; for example, through the use of renewable energy sources [4,5] and the need to prevent heat loss [6]. Lee et al. [7] determined a simple ground heat exchanger design capacity, while Park et al. [8] proposed optimal values of BHE spacing for typical irregular BHE cases using the GenOpt optimisation tool. An efficient energy consumption strategy must carry out advanced analyses of heat flow [9,10]. Such solutions are facilitated by computer simulations and the scale modelling of buildings [11]. Most of the tools available on the market anticipate the building's energy demands but do not provide microclimate simulations. Moreover, these tools need large amounts of data to do this [12,13]. In order to perform energy calculations, such as heat loss calculations from floors or basements, and to use the ground as a potential source for heat pump applications, information on ground temperatures is needed. Unfortunately, the performance of these models strongly depends on an accurate estimation of input factors.

Ground temperature depends on many factors, such as the structure and physical properties of the ground (volumetric heat capacity C , thermal conductivity λ , soil latent heat and moisture), changes in ambient temperature and other variables, as well as (to a greater or lesser extent) the characteristics of the ground surface (vegetation, slope orientation, etc.). Larwa [14] determined that the amplitude of the daily average solar radiation flux strongly affects the total amount of heat transferred between the subsoil

and the environment during the year, while other parameters have a negligible effect. Piotrowska-Woroniak [15] presented the phenomenon of thermal ground regeneration in the period between heating seasons, based on measurements from 22 September 2016 to 12 October 2020. The temperature of the ground surface is affected by complex processes of convection and radiation in its immediate surroundings and further out, as well as energy loss due to evaporation and heat transfer between the surface and deeper layers of the ground [16,17]. In addition, the temperature of the ground at a given point depends on its depth beneath the ground surface. Depending on the depth, three ground temperature zones can be distinguished: the near surface zone (surface temperature), the shallow zone (subsurface temperature) and the deep zone. In the near surface zone, the temperature is strongly influenced by the daily fluctuations of the surface ground temperature, depending on weather conditions. In addition, other meteorological factors, such as wind and rain, can cause significant local variations. In the shallow zone, ground temperature depends on seasonal fluctuations and is close to the average annual air temperature. In the deep zone, ground temperature remains almost constant and increases very slowly with depth, depending on the local value of the geothermal gradient [18,19]. The influence of the frost heave of soils has been studied by Zięba et al. [20].

The exact determination of temperature distribution in the ground (especially surface temperature, for which temperature changes are considerable) is not easy. The results of ground temperature measurements in various conditions have been presented by other scientists [21,22]. Popiel et al. [23] presented temperature distributions measured in the ground in Poland from summer 1999 to spring 2001. Le et al. [24] presented a measurement model, the distribution profiles of temperature, and a preliminary assessment of geothermal potential at depths of 0.1–3.6 m in eastern China. Marshalko et al. [25] determined the connections between engineering and geological zones and landscape elements in the Czech Republic. Ground temperature in the near surface and shallow zones has been studied in detail and described in [26–28]. Based on the measurement results, models describing the temperature in the ground have been developed. They comprise analytical models (e.g., [17,19,27]), semi-analytical models (e.g., [19,29]), numerical models in 1D, 2D or 3D states (e.g., [16,26,30]) and empirical models, as well as models based on artificial neural networks (e.g., [31]). Mihalakakou et al. [32] developed a model for forecasting daily and annual changes in the earth's surface temperature based on ten-year hourly temperature measurements for bare earth and short grass coverage in Athens and Dublin. The comparison of eight mathematical models for the prediction of ground temperature (the models predicting ground temperature) was carried out by Michopoulos et al. [28]. Tong et al. [33] developed a numerical model for predicting ground temperature in China. The analyses took into account the influence of short-wave solar radiation, long-wave radiation, latent evaporation energy, heat conduction, heat convection, soil freezing and thawing. Serageldin et al. [34] developed an analytical model to predict the profile of soil temperature distribution, based on six different new cities in different areas in Egypt with four different ground surface cover conditions. They obtained error and correlation coefficient values between their analytical and empirical results of 5.59% and 98%, respectively. Among the available models, due to a relatively simple application and the speed of calculations, the most frequently used analytical models are the semi-infinite solid model and the sinusoidal model. The sinusoidal model has been implemented in most simulation programs, i.e., EnergyPlus [35], DOE-2 [36] and TRNSYS [37], to predict ground temperature distribution. The availability of the method depends on the availability of input data. In order to calculate heat losses through building envelopes, especially those in contact with the ground, simplified analyses are used. The flow of heat through building envelopes is analysed in a steady state, and the thermal resistance method is used to describe the processes taking place. Such simplifications are considered acceptable due to the insignificant share of heat losses to the ground in the entire thermal balance of the building (10–15% in the case of heat losses through basements and foundations and 10% through slab-on-ground structures [38]), the heat flux density distribution [39] and the accuracy resulting from the transformation of three-dimensional tasks into two-dimensional ones [40].

Moreover, the methodology for calculating heat loss by penetration through the ground specified in ISO 13370 [40] introduces a number of simplifications, such as the shape of building projections and characteristic dimensions. The approach presented in the ISO standard assumes pure conduction heat transfer with uniform thermal properties and sinusoidal boundary conditions [23]. In reality, however, the calculation of heat loss from a building to the ground is a complex task, heat conduction being three-dimensional and non-stationary.

Heat loss to the ground has been the subject of many analyses. Borelli et al. [41] presented various forms of nodes in the connection system—a foundation slab with a foundation wall—in the context of changes in linear heat loss coefficients. Pawłowski [42] presented an analysis of a material solution for ground flooring with respect to the new heat and humidity requirements. He calculated the thermal bridge, which is the effect of connecting the foundation wall with the slab (linear coefficient of heat loss λ (W/mK). Medved and Cerne [43] developed their own method of estimating heat loss to the ground based on the so-called weight factor F_g . Abdul-Jabbar [44] analysed four methods of defining heat loss to the ground depending on the geometry of building projections and the depth of foundations. Kang et al. [45] presented a novel co-simulation method of dynamic underground heat transfer with building energy modelling (based on an equivalent slab model).

Henriksson [46] demonstrated that the area of heat loss through a floor surface can be divided into two zones: an internal zone located in the central part of the building, which is not influenced by the temperature of the external environment (Q_1), and an external zone, which comprises the area around the external walls with a width of 0.75 m, in which heat loss fluctuates depending on the changes in outside air temperature (Q_2). These observations are especially important in the case of a shallow foundation depth of buildings (below 1.0 m), where the foundations are made as benches. This principally applies to single-family houses, bungalows or single-storey houses with an attic and a usable area of approx. 100 m². A trend of building such houses has become more and more evident in Poland due to the reduction of construction and operation costs, as well as generational changes (a house serves one generation for half of its life). Shallow foundations are also used for lightweight solutions, e.g., modular construction and domes [47]. In addition, with zero-emission houses, it is necessary to reduce or eliminate heat loss through the floor, including the places where the vertical envelope joins the floor on the ground, which has not been fully studied yet. The prediction of ground temperature is an important part of the computer simulations for the assessment of the energy consumption of buildings and efficient energy consumption strategies. Hence, there is a need to improve models describing the temperature in the ground, based on the results of systematically conducted in situ measurements, especially in the era of climate change (in winter 2020/2021 it was observed that, in Poland, temperatures dipped below 0 °C several times in a few weeks). This is related to the behaviour and parameters of soils; e.g., the permeability coefficient on samples after ten cycles of freezing and thawing was presented by Zięba et al. [48].

Based on the above, it can be observed that in the era of energy-saving solutions, the existing calculation methods for heat loss to the ground are still based only on the average temperature of the external and internal environment [40]. Therefore, the aim of the article is to assess the effect of the real ground temperature on a building's heat loss. For this purpose, numerical analyses and in situ measurements of soil temperature profiles in Poland for real conditions under a residential building and in the ground (outside the building) were performed. The proprietary geometric model of the partition was proposed based on the measurements obtained on the test stand. This assessment is carried out using the methodology and geometric model for the elements in contact with the ground specified in ISO 10211 [49]. Due to the fact that the highest heat losses are observed in the wall strip, the analysis focused on the detail connecting the slab on the ground with the external wall. In the era of changing weather conditions, the obtained results are a valuable contribution in terms of their impact on the assessment of the consumption of energy in urban contexts. Heat and mass transfer are not considered in this study.

2. Methodology

2.1. Subject of Analysis

The subject of the study was a single-family building with a development area of approximately 155 m². The building is located directly on the foundation benches at a depth of 0.7 m below the ground surface. The 0.3 m × 0.4 m wide benches are made of C16/20 class concrete reinforced with B500SP steel rods. The walls were made as sandwich panels from reinforced concrete class C20/25, 0.1 m thick, and with thermal insulation, 0.1 m thick [47].

The spaces between the benches were filled with sand to a depth of about half of the height, followed by lightweight concrete with a density of 900 kg/m³.

The subsoil was made up of sand of various fractions to a depth of 2.0 m.

2.2. Methodology of In Situ Research

The temperature of the native soil and the embankment soil was measured. The measurement was made at various depths from 0 to approximately 2 m for six consecutive months (from 1 May to 31 October). The temperature was measured along the depth of the subsoil in the following periods:

- 1 May–30 June, when only the flooring on the ground was laid, in 17 points;
- 1 July–31 October, when the entire building envelope was completed, in 8 points.

The temperature was measured in two profiles (see Figure 1):

- Profile I, located under the building at a depth of −0.05, −0.25, −0.45, −0.65, −0.85, −1.05 and −1.25 m from the foundation depth;
- Profile II, located in the area outside the building at a depth of −0.15, −0.35, −0.55, −0.75, −0.95, −1.15, −1.35, −1.55, −1.75 and −1.95 m from the ground surface.

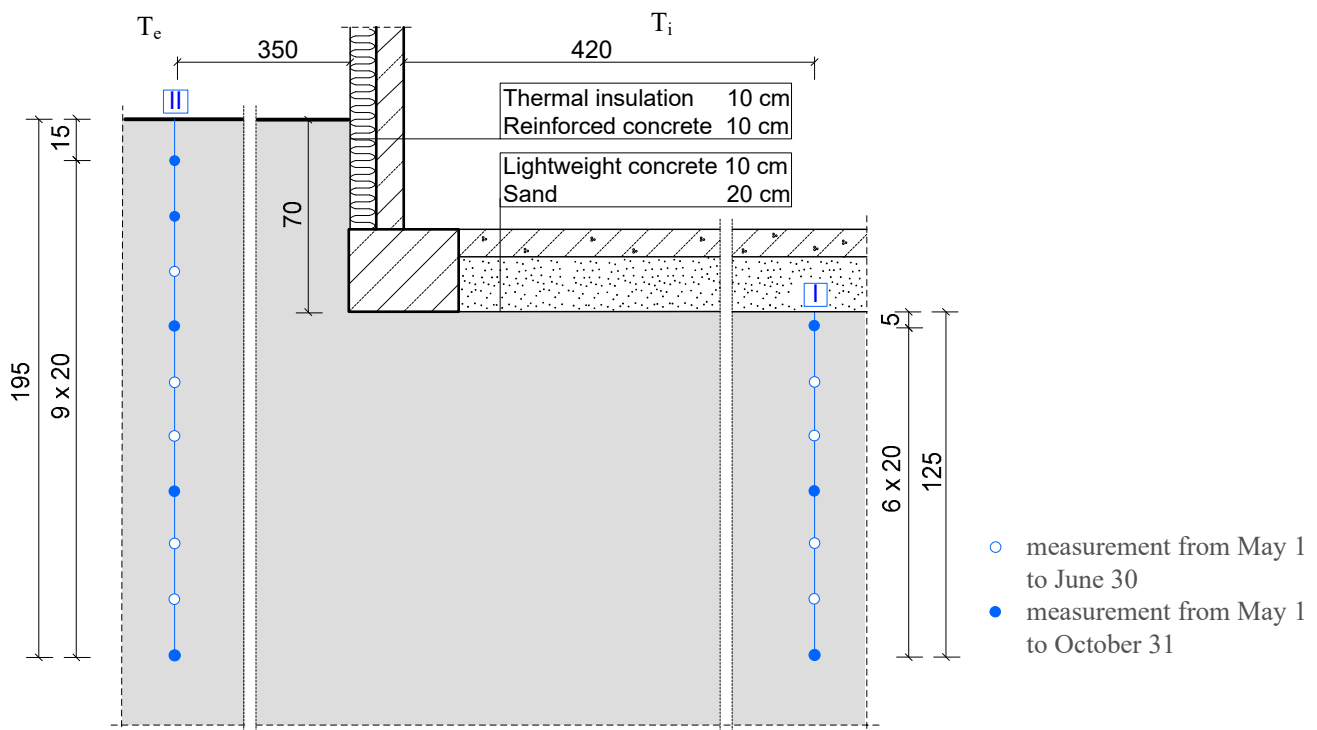


Figure 1. Schematic of the arrangement of temperature sensors.

Temperature distribution in the ground was measured using a multi-channel, automatic measurement system. Temperature measurements were made with YSI 44,005 thermistors with a measuring range from −40 to +105 °C and a measurement accuracy of 0.5 °C. The tem-

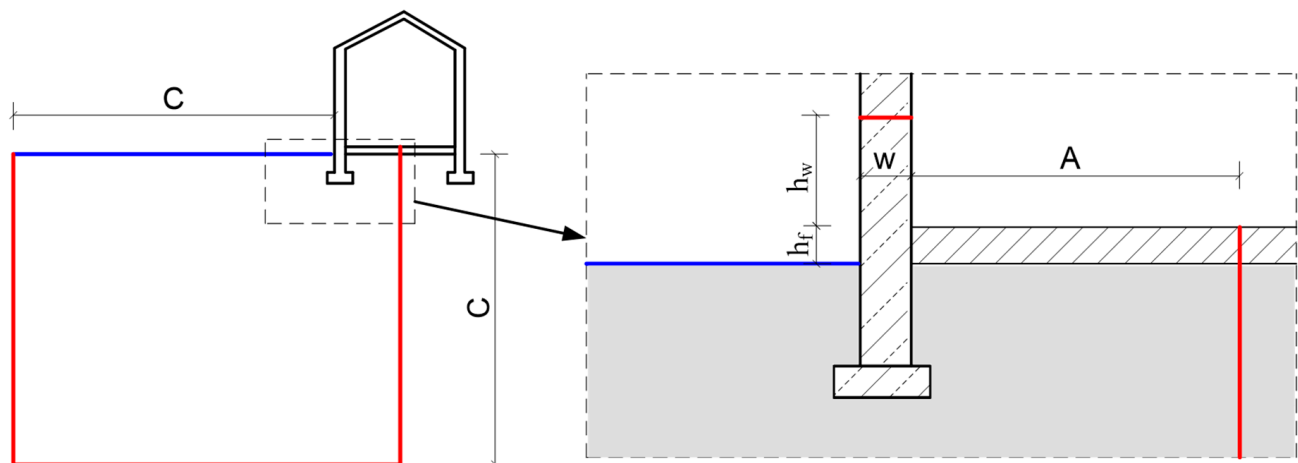
perature sensors were connected to Geokon 8002 multi-channel recorders. The measurements were recorded every hour.

The outside air temperature was measured on a test stand at the Faculty of Civil Engineering of the Silesian University of Technology in Gliwice (i.e., at a distance from the test site). The measurement was performed using the Ahlborn FMA510H meteorological multi-sensor with a temperature measurement range from -52 to $+60$ °C \pm 0.1 K [47,50].

2.3. Methodology of Numerical Analysis

The calculations were carried out using the finite element method (FEA) in the THERM program [51]. Two-dimensional heat flow was modelled.

The calculation of heat loss by the elements in contact with the ground was made on the basis of the geometric model given in ISO 10,211 [49]. In the base model, adiabatic limits were adopted in accordance with the assumptions shown in Figure 2. In subsequent analyses, the temperature distribution was adopted in accordance with actual measurements, as presented in the diagram below. At the ground surface, the external air temperature T_e was adopted.



$$A = \min\{0.5 \times b; 4 \text{ m}\}$$

$$C = \min\{2.5 \times b; 20 \text{ m}\}$$

$$h_w = \max\{3 \times w; 1 \text{ m}\}$$

b – floor width

— adiabatic boundary conditions
— ground level

Figure 2. Geometry of the model.

The following calculation variants were analysed:

- (1) Base model (based on the assumptions of ISO 10211 [49]): geometric model in compliance with the standard [49]; $T_i = 20.0$ °C; boundary conditions adopted for the month of October:
 - Variant W_1: $T_e = 9.3$ °C, average monthly temperature of a typical meteorological year TMY [52], temperature of the ground surface $T_{gr}(0.00 \text{ m}) = T_e$; below the ground surface, adiabatic temperature distribution (at the depth and width C);
- (2) Models based on the reliable model: changed model geometry—the dimension C in the geometric model was changed to the real value, i.e., 1.95 m; the temperature at a depth of 1.95 m was adopted, $T_i = 20.0$ °C; boundary conditions were adopted for the month of October:
 - (2a) For Profile I:

- Variant W_2: T_e measured external air temperature, ground surface temperature $T_{gr}(0.00\text{ m}) = T_e$, $T_{gr}(1.95\text{ m})$ temperature measured at a depth of 1.95 m in Profile I;
- Variant W_2a: T_e measured external air temperature, $T_{gr}(0.00\text{ m})$ measured ground temperature near the surface, $T_{gr}(1.95\text{ m})$ temperature measured at a depth of 1.95 m in Profile I.

(2b) For Profile II:

- Variant W_3: T_e measured external air temperature, ground surface temperature $T_{gr}(0.00\text{ m}) = T_e$, $T_{gr}(1.95\text{ m})$ temperature measured at a depth of 1.95 m in Profile II;
- Variant W_3a: T_e measured external air temperature, $T_{gr}(0.00\text{ m})$ measured ground temperature near the surface, $T_{gr}(1.95\text{ m})$ temperature measured at a depth of 1.95 m in Profile II.

Heat conductivity indexes of the materials used in the calculations are presented in Table 1.

Table 1. Properties of materials.

Material	Heat Conductivity Index λ (W/m·K)
Reinforced concrete	1.700
Thermal insulation	0.027
Lightweight concrete	0.097
Sand	2.000

The percentage accuracy of the calculation error (maximum error energy norm) was adopted at 5% and the number of iterations (maximum iterations) was equal to ten.

Then, the verification calculations were performed using the PsiTherm program. The analysed node was treated as a 3D connection. The material assumptions were taken from Table 1. The geometry of the connection was built according to the assumptions of the standard EN ISO 10211 (variant W_1; Figure 3) and individual assumptions for the variant W_2 and W_3 (Figure 4).

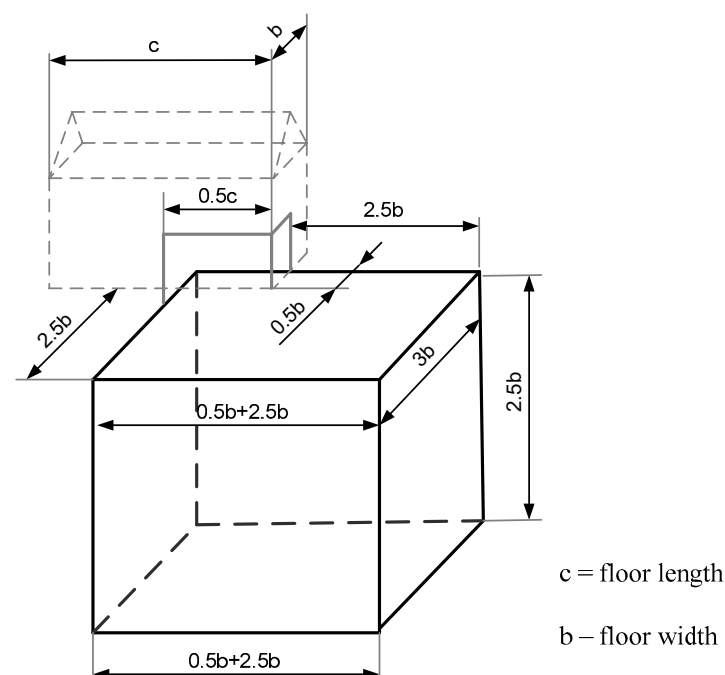


Figure 3. Geometry of the 3D model.

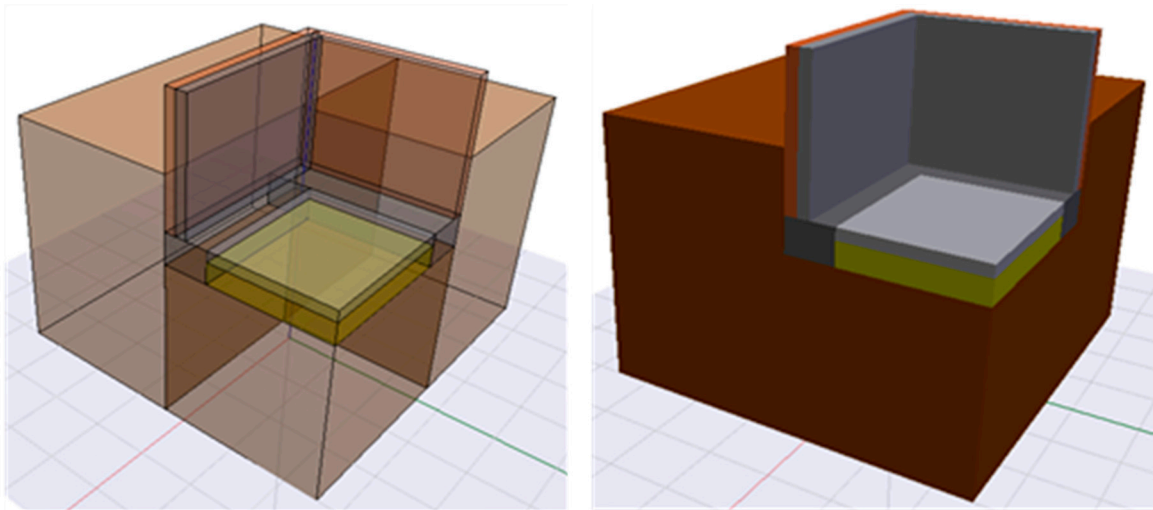


Figure 4. Geometry of the model adopted in the calculations—an example for variants W_2, W_2a, W_3, W_3b.

With each calculation, the value of the average heat flux through the internal surfaces for the analysed detail was determined.

3. Results and Discussion

3.1. Measurement Results

Figure 5 presents the course of ground temperature in time at different depths under the building (Profile I) and outside the building (Profile II). For Profile I, the obtained temperature range was from 9.0 to 19.1 °C and for Profile II it was from 6.7 to 28.1 °C. It can be observed that the distribution of ground temperature under the building is more homogeneous than that outside the building. Moreover, for the first distribution, hourly temperature changes are not so high as observed for the temperatures of ground unshielded by the building.

Moreover, the variation in hourly temperature values decreases with depth. This is also confirmed by the results of ground measurements obtained by Xu and Spitler [53], who obtained a flatter distribution of temperatures measured in time for the depth of 1.0 m than for the depth of 0.5 m.

Figure 6a,b present changes in average daily ground temperature along the depth for individual months (marked with respective colours). This is confirmed by lower variation in the daily temperature range (lower temperature range) over a month for the ground located under the building compared to the ground temperature distribution in the area outside the building at the same depth (see the dashed line in Figure 6). In colder months (October), higher temperatures were obtained for the ground under the building than for the ground outside the building, yet the opposite was true for the warmer summer months (July, August), when lower temperatures were observed in the profile under the building. It is surprising that the highest temperatures in the profile under the building were obtained in September.

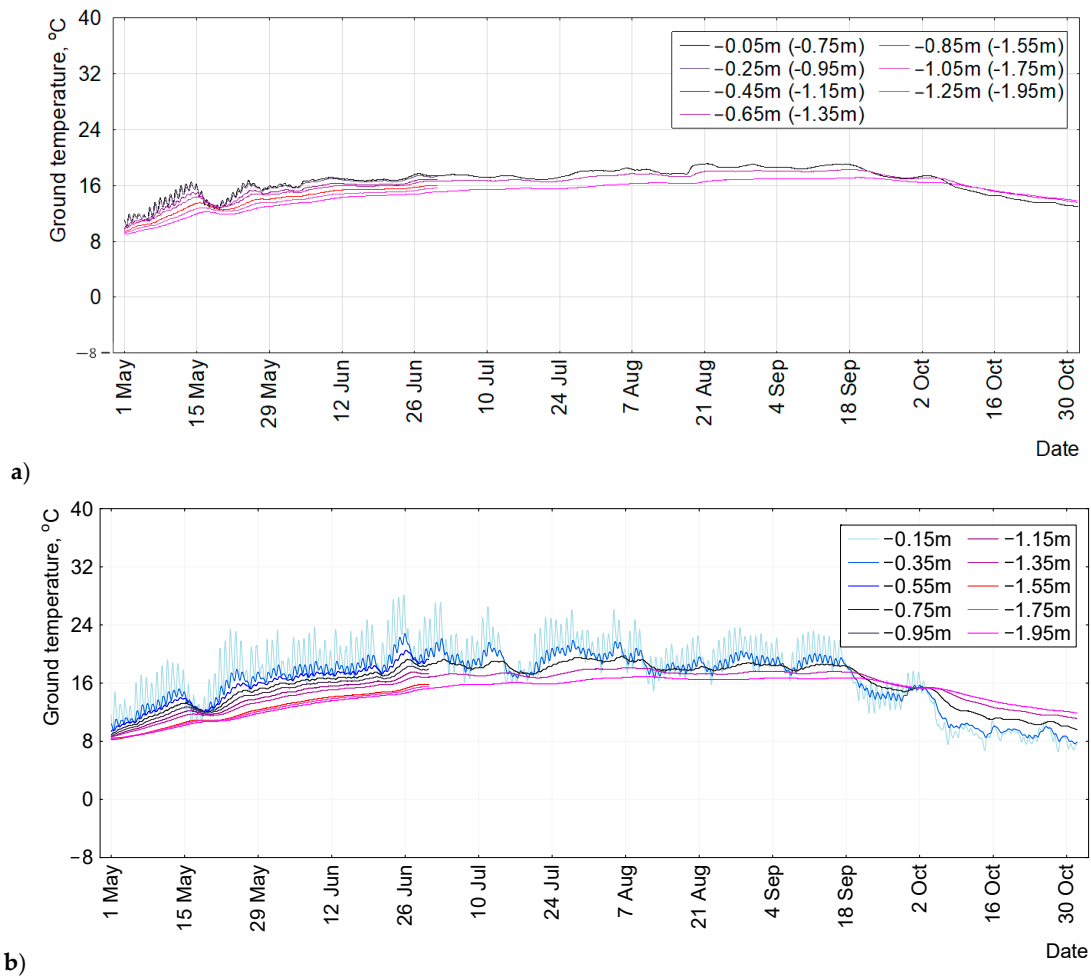


Figure 5. Hourly ground temperatures at various depths; 1 May–31 October: (a) Profile I; (b) Profile I.

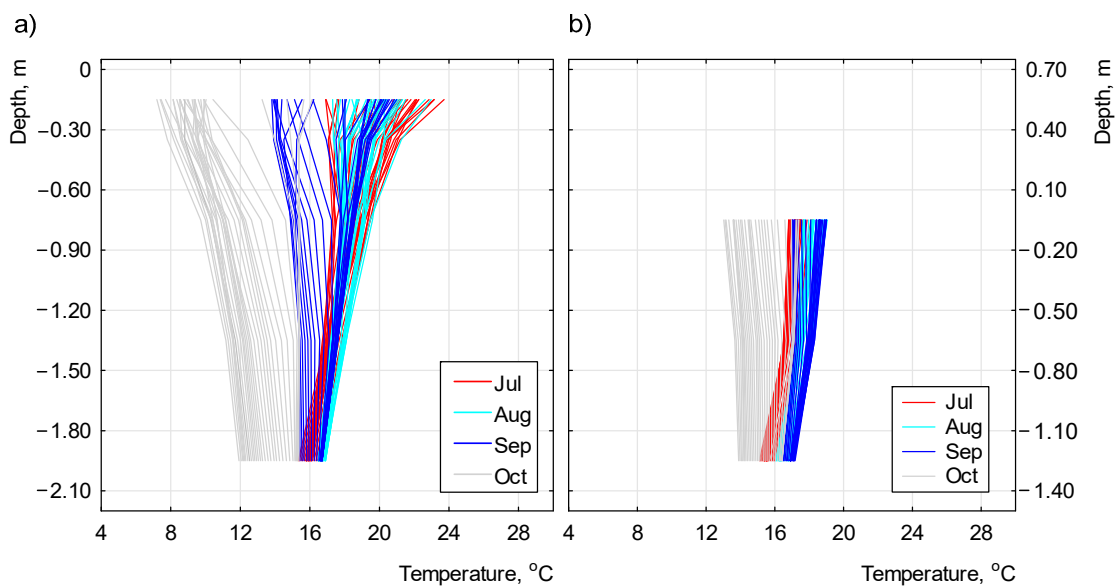


Figure 6. Daily average ground temperature profiles at various depths, 1 July–31 October: (a) Profile II; (b) Profile I.

Based on a comparison of the measured ground temperature results to the outside air temperatures (Figure 7), it can be observed that the maximum temperatures in September are similar to the maximum temperatures in August and are lower than the maximum temperatures in July. The number of higher amplitudes in September, however, is greater than that in August, and the said month was also preceded by warmer months, so in the months preceding September the ground was heating up, reaching the highest temperatures in the profile under the building in September. The ground temperature also did not drop immediately in response to the decrease of external temperatures, as the building shielded the ground against the direct impact of air temperature. Moreover, the said observation speaks for the accumulation of heat over a certain period (heat capacity of the ground).

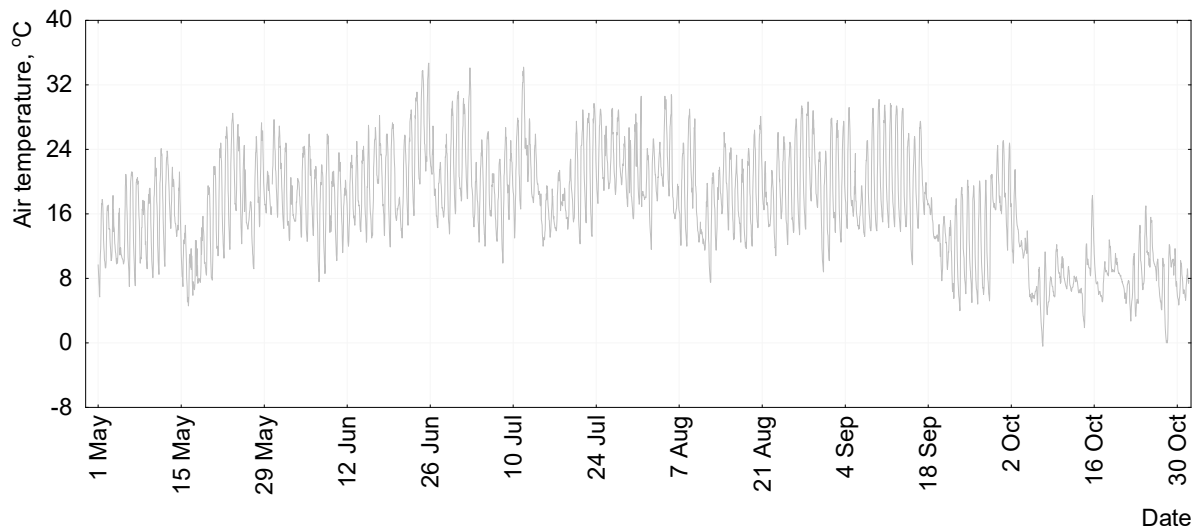


Figure 7. External air temperature, 1 May–31 October.

A higher impact of external temperature on the obtained temperature distribution in the ground was observed for the unshielded area (Profile II). The course of the outside air temperature is presented in Figure 7 and the average monthly temperatures in Table 2.

Table 2. Properties of materials.

	Monthly Average Temperature (°C)			
	July	August	September	October
External air	20.6	19.3	17.1	8.7

The changes of average monthly temperature along the depth for Profiles I and II are presented in Figure 8a,b, respectively. It can be observed that the large thermal mass of the ground results in a slow reaction to the changes in temperature fluctuations in the outside air. The high amplitude of the outside air temperature fluctuations is dampened according to the depth. The amplitude of ground temperature in Profile I (under the building) is lower.

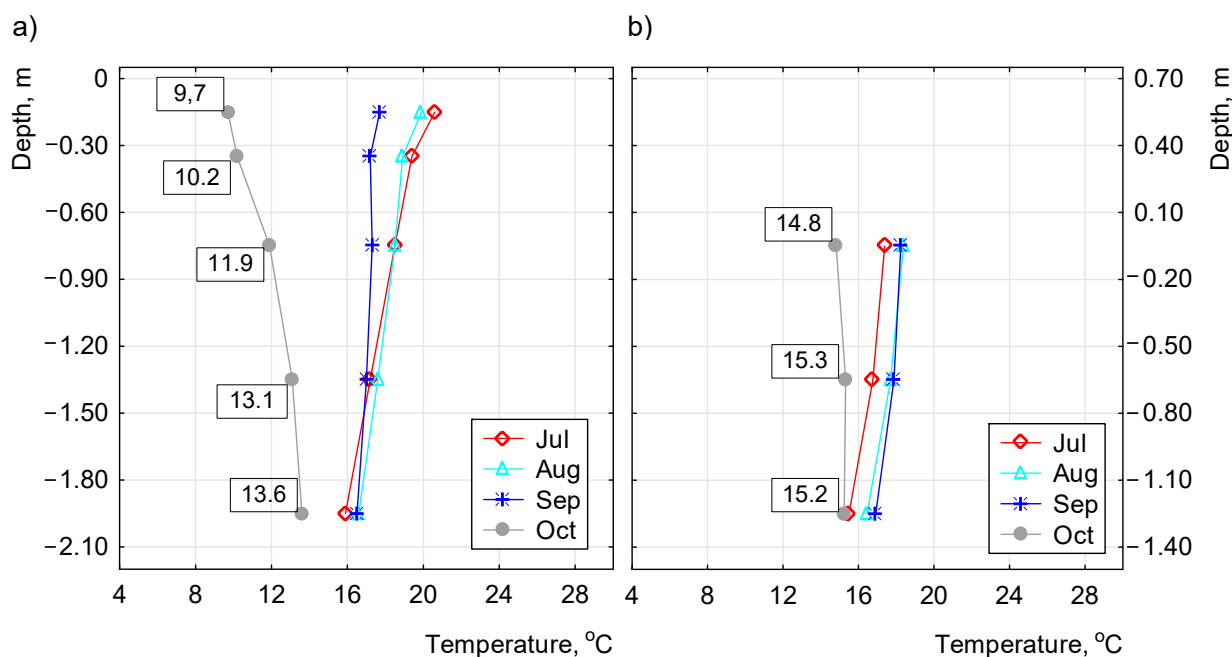


Figure 8. Monthly average ground temperature profiles at various depths, 1 July–31 October: (a) Profile II; (b) Profile I.

The monthly average ground temperatures were compared with the average outside air temperature (Table 2). It can be observed that ground temperatures directly beneath the ground surface were almost in phase with air temperatures and their values were close to the average air temperatures, which corresponds with the near surface zone [18,19]. The spread of ground temperature decreases with the depth (Figure 6). This is in line with the observations of other scientists [54]. Moreover, the maximum and minimum ground temperatures occur later than the corresponding air temperatures (the maximum or minimum occurs later than the corresponding temperature at the surface). The same phenomenon was observed by Florides and Kalogirou [54], who found that the maximum temperature of the ground at a depth of 2–3 m under the surface occurs about 5–6 months later than the average maximum temperature of the surface for calcareous sandstone and in situ mari [55]. Moreover, this is in line with the correlation obtained by Kasuda and Archenbach [56].

In the present study, it was demonstrated that the ground temperature change at a depth of more than 1.25 m below the ground level for a given month is less than 1% (Figure 8a), which proves its stability and the lack of impact of the outside air temperature. At a depth of 1.25 m below the foundation (1.95 m below ground level for the area where the building is located), no influence of the outside air temperature on the ground temperature was found (Figure 8b).

The strength of the interdependence between air temperature and ground temperature at successive measurement points for Profiles I and II was described with determination coefficients as a measure-of-fit quality of the model. Assuming that the coefficient of determination defines the percentage extent to which one variable explains the variability of the other, we can conclude the following:

- A decrease of the strength of interdependence between the variables (outside air temperature and ground temperature at a given depth) was observed with growing measurement depth. In other words, this means that the impact of outside temperature disappears with the depth (R^2 from 0.760 to 0.342; a logarithmic decrease-of-fit coefficient was observed with growing depth).
- Outside air temperature exerts a smaller impact on ground temperature under the analysed building (R^2 equal to about 0.080–0.364).

3.2. The Results of Numerical Analyses

The conducted analyses were performed for stationary conditions, with October adopted as a representative month. The selected monthly average temperatures were used in the numerical analyses (see Table 3). The analyses were performed for five calculation variants in accordance with Section 2.2.

Table 3. Temperatures adopted in the calculations.

Model	Variant	Internal Air Temperature T_i (°C)	External Air Temperature T_e (°C)	Surface Ground Temperature $T_{gr}(0.00\text{ m})$ (°C)	Ground Temperature at a Depth of 1.95 m $T_{gr}(C)/T_{gr}(1.95\text{ m})$ (°C)
Base model	W_1	20	9.3 °C	T_e	Adiabatic
Reliable model	W_2 Profile I	20	8.7 °C	T_e	15.2
	W_2a Profile I	20	8.7 °C	9.7	15.2
	W_3 Profile II	20	8.7 °C	T_e	13.6
	W_3a Profile II	20	8.7 °C	9.7	13.6

Figures 9 and 10 present the results of the numerical analyses for monthly average temperatures. At the intersection of the foundations and the wall, we can see the highest concentration of isotherms, regardless of the adopted boundary conditions (temperatures). The isotherms form a convergent bundle of lines at this point. As the distance from the partition increases, the isotherms occur less frequently in the base model (Figure 9a) than in the other two models (Figure 9b,c). According to the assumption, this is an adiabatic distribution. For the reliable models (Figure 9b,c), we observe the dilution of isotherms at a distance of 1.0 m from the partition, followed by a parallel horizontal run of the isotherms. Despite the adoption of different temperatures on the ground surface and at a depth of 1.95 m (the bottom of the model) in the reliable models (Figure 9b,c), no changes in the distribution of isotherms or in their values were observed. This is probably related to slight differences in the adopted temperatures at the edges of the model (the difference of 1.0 °C for ground surface temperature and the difference of 1.6 °C for ground temperature at a depth of 1.95 m).

The heat flux density lines are perpendicular to the isotherms (see Figure 10). In each case, the highest heat flux density was obtained at the joint between the outer wall and the foundation. Then, the heat flux density decreases with the increasing distance from the outer wall. The distribution of fluxes in terms of quality, however, is different. Therefore, based on heat flux distribution, it can be concluded that the most vital place in terms of heat loss through the partition and foundation is the connection point between the wall and the foundation, regardless of the adopted distributions of ground temperature with growing depth. The highest values were obtained for the base model, and the area in which they occur was significantly smaller than that for the reliable models with limited dimensions. For the reliable models, lower heat flux was observed, and thus lower heat losses through the partition and through the slab-on-ground structure. This means that, based on the temperatures of a typical meteorological year (TMY), the obtained results are on the safe side.

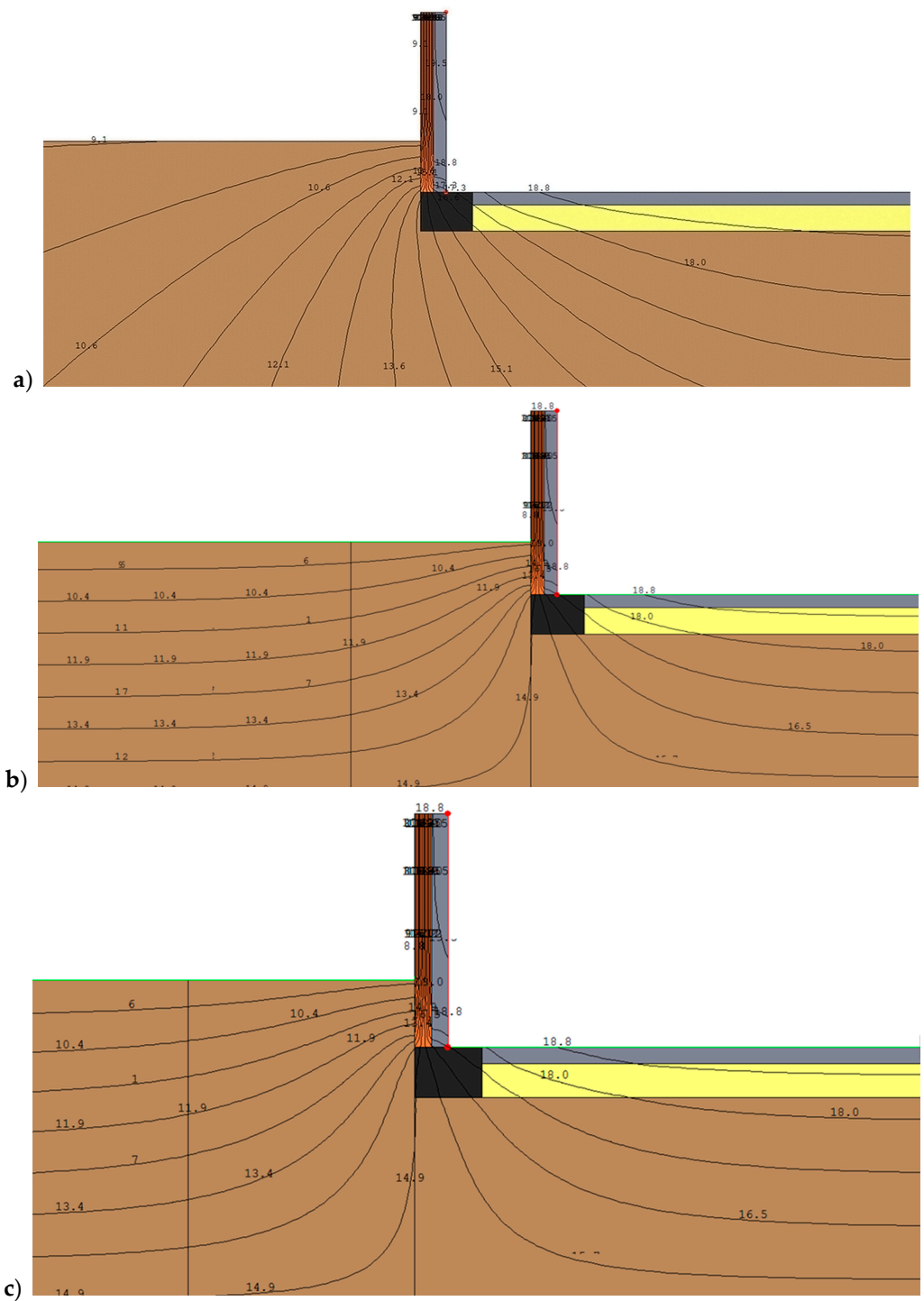


Figure 9. Distribution of isotherms: (a) base model W_1; (b) model W_2 for Profile I; (c) model W_3 for Profile II.

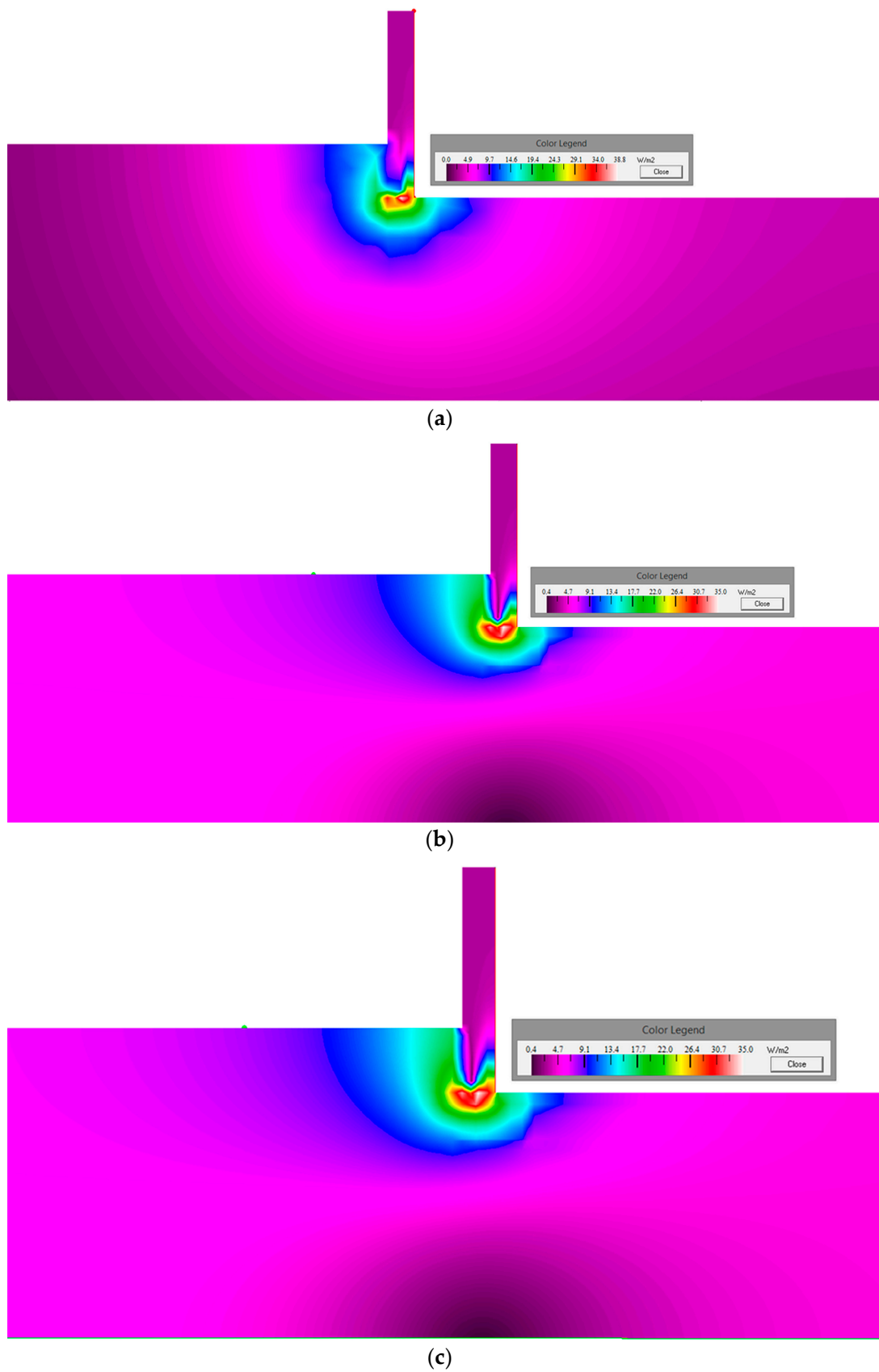


Figure 10. Heat flux density distribution: (a) base model W_1 ; (b) model W_2 for Profile I; (c) model W_3 for Profile II.

Figure 10 shows changes in the heat flux density at the edges of the analysed system. The aim of the numerical analyses was to indicate differences in heat flow, which are a consequence of the simplification of the geometric model from the typical soil model (depth of $2.5b$, where: b = the width of the building; according to EN ISO10211 [49]) to the model with a limited depth up to about 2.00 m (Figure 2).

Heat flux and the corresponding heat flow per 1 m^2 was determined for each of the variants. The analysis was performed for the entire wall–foundation system (Table 4) and for the slab-on-ground structure alone (Table 5).

Table 4. Summary of the results of the numerical analysis for the wall–foundation system.

Parameter	Base Model	Reliable Model			
		Profile I		Profile II	
	W_1	W_2	W_2a	W_3	W_3a
Heat flux (W)	28.5	29.90	29.19	36.76	35.95
Heat flow (W/m^2)	5.50	5.88	5.72	7.20	7.04

Table 5. Summary of the results of the numerical analysis for the slab-on-ground structure.

Parameter	Base Model	Reliable Model			
		Profile I		Profile II	
	W_1	W_2	W_2a	W_3	W_3a
Heat flux (W)	20.61	22.68	22.20	29.03	28.54
Heat flow (W/m^2)	5.57	6.13	6.00	7.84	7.71

The obtained results refer to the entire detail, i.e., to the joint between the wall and the slab-on-ground structure, modelled in accordance with the guidelines of the standard [49].

It can be observed that the results obtained in the numerical analyses with the use of the basic geometric model (Variant W_1) are consistent with the results obtained in the reliable model based on temperature profiles under the building (Variant W_2/W_2a, Profile I). The heat flux and heat flow results obtained for the reliable models are 4.9% and 6.9% higher compared to the base models for the wall–foundation system, and 10.0% and 10.1% higher for the slab-on-ground structure for Variant W_2 (Profile I). For Variant W_2a (Profile I), however, the results are higher by 2.4% and 4.0% for the wall–foundation system, and by 7.7% and 7.7% for the slab-on-ground structure. The adoption of temperatures from the area outside the building as the boundary condition (Profile II) results in higher differences between the obtained results of the numerical analyses. The difference in heat flow obtained in the numerical analyses for Profiles I and II is about $2 \text{ W}/\text{m}^2$, for both the calculations for the wall–foundation system (Table 5) and the slab-on-ground structure (Table 6). Moreover, the adoption of temperatures for the ground outside the building leads to the overestimation of the heat flux calculation, which is caused by lower temperatures in the particular layers of the ground.

Table 6. Heat flux in the analysed 3D connection for all tested cases.

Parameter	Base Model	Model			
		Profile I		Profile II	
	W_1	W_2	W_2a	W_3	W_3a
Heat flux (W)	46.1	49.01	45.06	49.81	45.79

Table 6 shows the calculation results for the analysed 3D connection for all tested cases. Figure 11 presents the distribution of isotherms for variants W_2, W_2a, W_3 and W_3a.

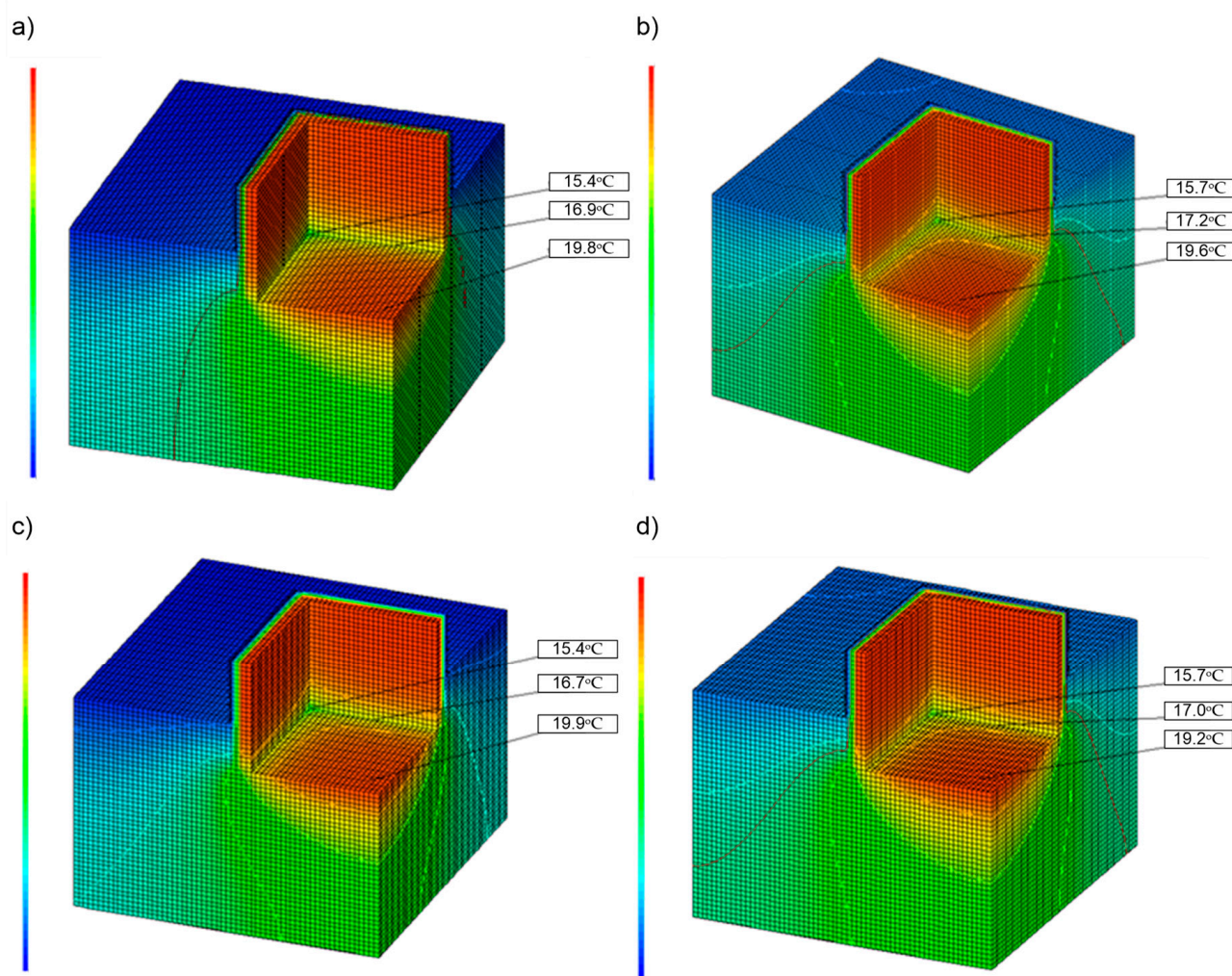


Figure 11. Temperature field changes for a 3D node of the foundation–wall connection with a slab: (a) model W_2, (b) model W_2a for Profile I; and (c) model W_3, (d) model W_3a for Profile II.

Numerical modelling in the PsiTherm program (treating the connection as a 3D node) did not show significant differences in the distribution of the temperature field on the partition surface (Figure 11) or in the heat flux values (Table 6) between the analysed variants. It was found that the ground temperatures, which change at a depth of 1.95 m (depending on the buildings located above them or the lack thereof), do not substantially affect the temperature distribution profile on the surface of the elements and the heat losses. Simplifying the geometry of the model (variants W_2 and W_3) and reducing the soil depth to about 2.0 m are not a source of additional discrepancies in the obtained results.

The main goal of this study was to explore initial diagnostics of heat loss depending on adopted temperature profiles. In addition, the typical soil model was abandoned. The dimension of the ground to a depth of $2.5b$ (where b = the width of the building) was limited to a depth of about 2.0 m. The adopted ground model for this study, i.e., the model of building foundation, provides results similar to the values obtained for the model of the ISO 10211 standard [49]. Therefore, the calculations of heat loss can be reduced to simple models with limited dimensions, thus eliminating the problem involving the adoption of fictitious adiabatic limits for the standard-specific depth of ground (ISO 10211 [49]). The performed numerical analyses refer to a steady state and take into account the heat transport model based on the principle of conduction in a soil medium with constant thermal properties. The algorithm used does not consider the complex processes of heat

and mass transport and their influence on the change of the hygrothermal state of the soil and partition materials.

4. Conclusions

The aim of the research was to assess the effects of soil temperature measured in situ on the heat loss analyses of a building. The profiles of ground temperature under and outside a building were measured. Based on the measurements obtained on the test stand, the authors proposed their own geometric model of the partition. The assessment was carried out using the methodology and geometric model for elements in contact with the ground as specified in ISO 10211 [49]. Based on the results of the experimental study, the following important conclusions can be drawn:

1. Henriksson's calculation model confirmed that the impact of floor slab insulation in its central area on thermal transmittance is small. The insulation of the wall strip, even with a low thickness of insulation material, gives a measurable effect in the form of reduced heat flow.
2. The research results presented for the representative period were used to develop the authors' own geometric model of a slab-on-ground structure, using the measured temperatures as boundary conditions.
3. As a result of using the measurements as boundary conditions, changes were obtained in the results of heat loss analyses compared to when the traditional boundary conditions based on a typical meteorological year (TMY) were adopted in the analyses. The heat flux and heat flow results obtained for reliable models are 4.9% and 6.9% higher compared to the base models for the wall–foundation system, and 10.0% and 10.1% higher for the slab-on-ground structure for Variant W_2 (Profile I). For Variant W_2a (Profile I), however, the results are higher by 2.4% and 4.0% for the wall–foundation system, and by 7.7% and 7.7% for the slab-on-ground structure. The adoption of temperatures from the area outside the building as the boundary condition (Profile II) results in higher differences between the obtained results of the numerical analyses. The difference in heat flow obtained in the numerical analyses for Profiles I and II is about 2 W/m^2 for both the calculations for the wall–foundation system (Table 5) and for the slab-on-ground structure (Table 6). The adoption of temperatures for the ground outside the building leads to overestimation in heat flux calculations, which is caused by lower temperatures in the particular layers of the ground.
4. Numerical modelling and treating the connection as a 3D node did not show significant differences either in the distribution of the temperature field on the partition surface (Figure 11) or in the heat flux values (Table 6) between the analysed variants.
5. The presented research results are preliminary studies, the purpose of which is to discuss the correctness of the available heat flow models involving the contact of buildings with the ground. In addition, as part of future research, it is planned to perform an analysis for an entire year and for non-stationary conditions.

Author Contributions: Conceptualisation, I.P.-S. and M.K.; investigation, I.P.-S. and B.O.-K.; data curation, I.P.-S.; formal analysis, M.K. and L.F.; methodology, I.P.-S., M.K., B.O.-K. and L.F.; resources, I.P.-S., M.K. and L.F.; software, I.P.-S. and B.O.-K.; supervision, M.K.; validation, M.K.; visualisation, I.P.-S. and B.O.-K.; writing—original draft preparation, I.P.-S., M.K. and B.O.-K.; writing—review and editing, M.K. All authors have read and agreed to the published version of the manuscript.

Funding: This research received no external funding besides statutory research of particular scientific units.

Institutional Review Board Statement: Not applicable.

Informed Consent Statement: Not applicable.

Data Availability Statement: Not applicable.

Conflicts of Interest: The authors declare no conflict of interest.

References

1. Directive (EU) 2018/2001 of the European Parliament and of the Council of 11 December 2018 on the Promotion of the Use of Energy from Renewable Sources, PE/48/2018/REV/1, OJ L 328. 21 December 2018. pp. 82–209. Available online: <https://eur-lex.europa.eu/eli/dir/2018/2001/oj> (accessed on 11 November 2021).
2. Directive 2009/28/EC of the European Parliament and of the Council of 23 April 2009 on the Promotion of the Use of Energy from Renewable Sources and Amending and Subsequently Repealing Directives 2001/77/EC and 2003/30/EC, OJ L 140. 5 June 2009. pp. 16–62. Available online: <https://eur-lex.europa.eu/legal-content/EN/ALL/?uri=CELEX%3A32009L0028> (accessed on 11 November 2021).
3. Pfeiffer, A.; Koschenz, M.; Wokaun, A. Energy and building technology for the 2000W society—Potential of residential buildings in Switzerland. *Energy Build.* **2005**, *37*, 1158–1174. [[CrossRef](#)]
4. Tsagarakis, K.P.; Efthymiou, L.; Michopoulos, A.; Mavragani, A.; Anđelković, A.S.; Antolini, F.; Bacic, M.; Bajare, D.; Baralis, M.; Bogusz, W.; et al. A review of the legal framework in shallow geothermal energy in selected European countries: Need for guidelines. *Renew. Energy* **2020**, *147*, 2556–2571. [[CrossRef](#)]
5. Florides, G.; Kalogirou, S. Ground heat exchangers—A review of systems, models and applications. *Renew. Energy* **2007**, *32*, 2461–2478. [[CrossRef](#)]
6. Măgurean, A.M.; Czumbil, L.; Manea, D.L.; Micu, D.D. Artificial intelligence based prediction model for the long-term heat flux losses through ground applied to large non-residential buildings. *Proc. Manuf.* **2019**, *32*, 434–441. [[CrossRef](#)]
7. Lee, S.-M.; Park, S.-H.; Jang, Y.-S.; Kim, E.-J. Proposition of Design Capacity of Borehole Heat Exchangers for Use in the Schematic-Design Stage. *Energies* **2021**, *14*, 822. [[CrossRef](#)]
8. Park, S.-H.; Jang, Y.-S.; Kim, E.-J. Using duct storage (DST) model for irregular arrangements of borehole heat exchangers. *Energy* **2018**, *142*, 851–861. [[CrossRef](#)]
9. Wonorahardjo, S.; Sutjahja, I.M.; Mardiyati, Y.; Andoni, H.; Thomas, D.; Achsani, R.A.; Steven, S. Characterising thermal behaviour of buildings and its effect on urban heat island in tropical areas. *Int. J. Energy Environ. Eng.* **2020**, *11*, 129–142. [[CrossRef](#)]
10. Andoni, H.; Wonorahardjo, S. A review on mitigation technologies for controlling urban heat island effect in housing and settlement areas. *IOP Conf. Ser. Earth Environ. Sci.* **2018**, *152*, 012027. [[CrossRef](#)]
11. Robinson, D. *Computer Modelling for Sustainable Urban Design: Physical Principles, Methods and Applications*; Earthscan Publications: London, UK, 2011.
12. Sola, A.; Corchero, C.; Salom, J.; Sanmarti, M. Multi-domain urban-scale energy modelling tools: A review. *Sustain. Cities Soc.* **2020**, *54*, 101872. [[CrossRef](#)]
13. Mutani, G.; Todeschi, V. Building energy modeling at neighborhood scale. *Energy Effic.* **2020**, *13*, 1353–1386. [[CrossRef](#)]
14. Larwa, B. Heat Transfer Model to Predict Temperature Distribution in the Ground. *Energies* **2019**, *12*, 25. [[CrossRef](#)]
15. Piotrowska-Woroniak, J. Assessment of Ground Regeneration around Borehole Heat Exchangers between Heating Seasons in Cold Climates: A Case Study in Białystok (NE, Poland). *Energies* **2021**, *14*, 4793. [[CrossRef](#)]
16. Staniec, M.; Nowak, H. The application of energy balance at the bare soil surface to predict annual soil temperature distribution. *Energy Build.* **2016**, *127*, 56–65. [[CrossRef](#)]
17. Badache, M.; Eslami-Nejad, P.; Ouzzane, M.; Aidoun, Z.; Lamarche, L. A new modeling approach for improved ground temperature profile determination. *Renew. Energy* **2016**, *85*, 436–444. [[CrossRef](#)]
18. Tsilingiridis, G.; Papakostas, K. Investigating the relationship between air and ground temperature variations in shallow depths in northern Greece. *Energy* **2014**, *73*, 1007–1016. [[CrossRef](#)]
19. Popel, C.O.; Wojtkowiak, J. Temperature distributions of ground in the urban region of Poznan City. *Exp. Therm. Fluid Sci.* **2013**, *51*, 135–148. [[CrossRef](#)]
20. Zięba, Z.; Witek, K.; Kilian, W.; Mońka, J.; Swierzko, R. Influence of Micro and Nanosilica on the Frost–Heave Process. *IOP Conf. Ser. Mater. Sci. Eng.* **2019**, *471*, 042020. [[CrossRef](#)]
21. Deru, M.P.; Kirkpatrick, A.T. Ground-Coupled Heat and Moisture Transfer from Buildings. In *Part 1: Analysis and Modeling. Part 2: Application Conference Paper, Proceedings of ASME 2001 Solar Engineering: International Solar Energy Conference (FORUM 2001: Solar Energy—The Power to Choose)*, Washington, DC, USA, 21–25 April 2001; The American Solar Energy Society: Washington, DC, USA, 2001. [[CrossRef](#)]
22. Van Manen, S.M.; Wallin, E. Ground temperature profiles and thermal rock properties at Wairakei, New Zealand. *Renew. Energy* **2012**, *43*, 313–321. [[CrossRef](#)]
23. Popiel, C.; Wojtkowiak, J.; Biernacka, B. Measurements of temperature distribution in ground. *Exp. Therm. Fluid Sci.* **2001**, *25*, 301–309. [[CrossRef](#)]
24. Le, A.T.; Wang, L.; Wang, Y.; Li, D. Measurement investigation on the feasibility of shallow geothermal energy for heating and cooling applied in agricultural greenhouses of Shouguang City: Ground temperature profiles and geothermal potential. *Inf. Processing Agric.* **2021**, *8*, 251–269. [[CrossRef](#)]
25. Marschalko, M.; Yilmaz, I.; Krčmář, D.; Cheng, X.; Kubáč, J.; Kycl, P. A small-scale map analysis of the engineering-geological zone and landscape element dependencies for the land-use planning purposes in the Czech Republic. *Environ. Earth Sci.* **2019**, *78*, 29. [[CrossRef](#)]
26. Naranjo-Mendoza, C.; Wright, A.J.; Oyinlola, M.A.; Greenough, R.M. A comparison of analytical and numerical model predictions of shallow soil temperature variation with experimental measurements. *Geothermics* **2018**, *76*, 38–49. [[CrossRef](#)]

27. Droulia, F.; Lykoudis, S.; Tsiros, I.; Alvertos, N.; Akylas, E.; Garofalakis, I. Ground temperature estimations using simplified analytical and semi-empirical approaches. *Sol. Energy* **2009**, *83*, 211–219. [CrossRef]
28. Michopoulos, A.; Papakostas, K.T.; Mavrommatis, T.; Kyriakis, N. Comparative assessment of eight models predicting the ground temperature. *JP J. Heat Mass Transf.* **2010**, *4*, 119–135. Available online: <https://ktisis.cut.ac.cy/handle/10488/14927> (accessed on 11 November 2021).
29. Yuan, Y.; Ji, H.; Du, Y.; Cheng, B. Semi-analytical solution for steady-periodic heat transfer of attached underground engineering envelope. *Build. Environ.* **2008**, *43*, 1147–1152. [CrossRef]
30. Xu, H.; Spitler, J.D. The relative importance of moisture transfer, soil freezing and snowcover on ground temperature predictions. *Renew. Energy* **2014**, *72*, 1–11. [CrossRef]
31. Mihalakakou, G. On estimating soil surface temperature profiles. *Energy Build.* **2002**, *34*, 251–259. [CrossRef]
32. Mihalakakou, G.; Santamouris, M.; Lewis, O.; Asimakopoulos, D. On the Application of the Energy Balance Equation to Predict Ground Temperature Profiles. *Sol. Energy* **1997**, *60*, 181–190. Available online: <https://eclass.upatras.gr/modules/document/file.php/ENV235/Gioulis10.pdf> (accessed on 11 November 2021). [CrossRef]
33. Tong, C.; Li, X.; Duanmu, L.; Wang, H. Prediction of the temperature profiles for shallow ground in cold region and cold winter hot summer region of China. *Energy Build.* **2021**, *242*, 110946. [CrossRef]
34. Serageldin, A.A.; Abdelrahman, A.K.; Ali, A.H.H.; Ali, M.R.O.; Ookawara, S. Soil temperature profile for some new cities in Egypt: Experimental results and mathematical model. In Proceedings of the 14th International Conference on Sustainable Energy Technologies, Nottingham, UK, 11–14 August 2015.
35. EnergyPlus. Available online: www.energyplus.net (accessed on 11 November 2021).
36. DOE2. Available online: www.doe2.com (accessed on 11 November 2021).
37. TRNSYS. Energy Simulation Software. Available online: sel.me.wisc.edu/trnsys/.1 (accessed on 11 November 2021).
38. Styronet. What Is the Percentage of Heat Loss from the Building? Available online: Styronet.pl/procentowa-utrata-ciepla-z-budynku.html (accessed on 11 November 2021).
39. Pogorzelski, J. A Heat Losses from Building via the Ground after PN-EN ISO 13370:2001. Building Research Institute—Quarterly. *Work. Build. Res. Instit. [Prace Instyt. Techn. Bud.]* **2002**, *3*, 21–43. Available online: <http://yadda.icm.edu.pl/baztech/element/bwmeta1.element.baztech-article-BTB2-0011-0109> (accessed on 11 November 2021).
40. *ISO 13370:2017 Thermal Performance of Buildings—Heat Transfer via the Ground—Calculation Methods*; International Organization for Standardization: Geneva, Switzerland, 2017.
41. Borelli, D.; Cavalletti, P.; Marchitto, A.; Schenone, C. A comprehensive study devoted to determine linear thermal bridges transmittance in existing buildings. *Energy Build.* **2020**, *224*, 110136. [CrossRef]
42. Pawłowski, K. Floor design in the light of new heat requirements. *Izolacje* **2014**, *1*, 26–33.
43. Medved, S.; Cerne, B. A simplified method for calculating heat losses to the ground according to the EN ISO 1370 standard. *Energy Build.* **2002**, *34*, 523–528. [CrossRef]
44. Abdul-Jabbar, N.K. Heat loss from below ground basements: Validation of some available methods. *Energy Convers. Manag.* **1999**, *40*, 1963–1977.
45. Kang, X.; Yan, D.; Xie, X.; An, J.; Liua, Z. Co-simulation of dynamic underground heat transfer with building energy modeling based on equivalent slab method. *Energy Build.* **2022**, *256*, 111728. [CrossRef]
46. Henriksson, R. *Warmeforluster Genom Golv Lagda Direct Pa Mark*; Meddelande: Lund, Sweden, 1959.
47. Pokorska-Silva, I.; Kadela, M.; Fedorowicz, L. A reliable numerical model for assessing the thermal behavior of a dome building. *J. Build. Eng.* **2020**, *32*, 101706. [CrossRef]
48. Zięba, Z.; Witek, K.; Mońka, J. The effect of micro- and nanosilica on the soil permeability coefficient under cyclic freezing and thawing conditions. *E3S Web Conf.* **2018**, *66*, 02004. [CrossRef]
49. *ISO 10211:2017 Thermal Bridges in Building Construction—Heat Flows and Surface Temperatures—Detailed Calculations*; International Organization for Standardization: Geneva, Switzerland, 2017.
50. Pokorska-Silva, I.; Kadela, M.; Fedorowicz, L. Variations of ground temperature in shallow depths in the Silesian region. *IOP Conf. Ser. Mater. Sci. Eng.* **2019**, *603*, 1757–8981. [CrossRef]
51. Windows and Daylighting. Available online: Windows.lbl.gov/therm-documentation (accessed on 11 November 2021).
52. Ministry of Development Funds and Regional Policy. Available online: www.archiwum.miir.gov.pl/stroony/zadania/budownictwo/charakterystyka-energetyczna-budynkow/dane-do-obliczen-energetycznych-budynkow-1/?fbclid=IwAR0dkKDgXOsETf2Bn2HzR_mCHGqh2a8cqV9f34dqiOsEIQxjCM-IGFDsv5E (accessed on 11 November 2021).
53. Xu, H.; Spitler, J.D. Importance of Moisture Transport, Snow Cover and Soil Freezing to Ground Temperature Predictions. In Proceedings of the 9th Nordic Symposium on Building Physics—NSB 2011, Tampere, Finland, 29 May–2 June 2011; Volume 1, pp. 163–170. Available online: https://hvac.okstate.edu/sites/default/files/pubs/papers/2011/05-Xu_and_Spitler_2011.pdf (accessed on 11 November 2021).

54. Florides, G.; Kalogirou, S. Annual Ground Temperature Measurements at Various Depths. In Proceedings of the CLIMA 2005, Lausanne, Switzerland, 9–12 October 2005. Available online: www.ktisis.cut.ac.cy/handle/10488/844 (accessed on 11 November 2021).
55. Florides, G.; Kalogirou, S. Measurements of Ground Temperature at Various Depths. In Proceedings of the 3rd International Conference on Sustainable Energy Technologies, Nottingham, UK, 28–30 June 2004. Available online: <https://www.semanticscholar.org/paper/Measurements-of-Ground-Temperature-at-Various-Florides-Kalogirou/3205b850d46eeaf53793f464059c8a7ac9af9661> (accessed on 11 November 2021).
56. Kusuda, T.; Archenbach, P.R. *Earth Temperature and Thermal Diffusivity at Selected Stations in the United States*; National Bureau of Standards Report. No. 8972; U.S. Department of Commerce National Bureau of Standards: Washington, DC, USA, 1965; Volume 71, p. 1. Available online: <https://nvlpubs.nist.gov/nistpubs/Legacy/RPT/nbsreport8972.pdf> (accessed on 11 November 2021).